Light Metals 2015
Edited by: Margaret Hyland
TMS (The Minerals, Metals & Materials Society), 2015

MONITORING LOCAL ALUMINA DISSOLUTION IN ALUMINUM REDUCTION CELLS USING STATE ESTIMATION

Yuchen Yao[1], Cheuk-Yi Cheung[1], Jie Bao*[1], Maria Skyllas-Kazacos[1]
[1]School of Chemical Engineering, University of New South Wales, Sydney, NSW, 2122, Australia

Keywords: Aluminum reduction, Alumina dissolution, Individual anode current, Kalman filter

Abstract

In the Hall-Héroult process, alumina dissolution rate is dependent on a number of process variables. One major variable is the superheat, especially in modern reduction cells which operate at low cell voltage. During the cell operation, routine practices and abnormalities give rise to energy imbalance at different parts of the cell, and consequently local superheat variations. This leads to variations in local alumina dissolution rate, and affects process efficiency and performance. This paper presents a method for monitoring local cell conditions by estimating the rate constant of alumina dissolution and alumina concentration using the extended Kalman filter. The method employs a combined mass balance and cell voltage model, which estimates the effective local superheat-dependent dissolution rate constant and local alumina concentration from individual anode current, cell voltage, alumina feed rate and anode-cathode distance. The results are verified with alumina concentration and superheat measured during an experiment conducted in an industrial cell.

Introduction

In the Hall-Héroult process, the dissolved alumina concentration is crucial and must be kept within a narrow range to avoid either the formation of sludge or the onset of anode effect [1]. A good control of dissolved alumina concentration largely depends on its feed regulation as well as the respective local dissolution rate. However, alumina dissolution rate is not easy to detect, and cell controllers can only regulate the overall dissolved alumina concentration by altering alumina feeding based on the variations of the pseudo-resistance curve. As the pseudo-resistance only reflects the combined effect of the resistance contributed by the overall dissolved alumina concentration and effective anode-cathode distance (ACD) across the cell, it therefore does not represent the spatial variations and local cell conditions. Thus, control strategies based on the pseudo-resistance do not provide a systematic way to account for the local dynamics of alumina dissolution. Furthermore, as the cell dimensions increase due to higher demand in productivity, spatial information that can be inferred from the pseudo-resistance becomes more diluted. As a result, cell monitoring using individual anode current measurements has attracted increasing attention from the industry as it can reflect local cell conditions. A number of applications have been proposed, which include signal based process monitoring [2-4], dynamic thermal modelling [5] and fault detection and diagnosis [5, 6].

Although the individual anode current is directly affected by local cell conditions such as the local dissolved alumina concentration and local ACD, it is difficult to separate one variable from another. As such, this paper proposes the use of Kalman filter to decouple and estimate local ACD, local alumina concentration as well as the respective dissolution rate based on a dynamic model that incorporates the dynamics of alumina dissolution and consumption. The estimation of localized cell condition using an extended Kalman filter has also been discussed in [7-9], in which a dynamic model has been employed to estimate the alumina concentration, yet the variation of local ACD was ignored. An improved Kalman filter structure has been proposed in [10] to estimate the localized ACD as a parameter and the local concentration of the dissolved alumina as a state assuming *constant* alumina dissolution rate. In this paper, the Kalman filter structure presented in [10] is further developed to include the estimation of alumina dissolution rate. It has been shown in [11] that the dissolution rate depends on a number of factors. In smelters operating at low cell voltage, the superheat becomes the dominant factor for alumina dissolution, as cold alumina can freeze the surrounding bath and forms agglomerate with a frozen shell of bath [12]. The alumina dissolution rate constant is then mainly dependent on the superheat. Thus the proposed method is capable of not only monitoring the concentration of the dissolved alumina, but also observing the superheat-dependent dissolution rate constant. The results will be compared with the superheat measurements obtained from an experiment where an excessive amount of cold alumina was fed into an industrial cell.

This paper is then organized as follows. The process model is presented in the next section, and is followed by a description of the formulation of the extended Kalman filter. The estimation results are compared with measured values. The paper concludes with discussion of the results and potential further development.

Process Modelling

In the Hall- Héroult process, the dissolution of alumina that enters the cell follows fast and slow mechanism with a specific weight ratio and different rate constants [13]. For instance, alumina powders dissolve relatively faster in contrast to the agglomerates. Therefore, the concentration of the three kinds of alumina that could co-exist in the bath is considered in this model, and is represented as c_1, c_2 and c_3. A nonlinear state-space model that relates dissolved alumina concentration and ACD to the cell voltage is developed with the following structure:

$$\begin{aligned}
\frac{\mathrm{d}c_1}{\mathrm{d}t} &= -k_1 \cdot c_1 + \frac{u}{M} \cdot r \\
\frac{\mathrm{d}c_2}{\mathrm{d}t} &= -k_2 \cdot c_2 + \frac{u}{M} \cdot (1 - r) \\
\frac{\mathrm{d}c_3}{\mathrm{d}t} &= k_1 \cdot c_1 + k_2 \cdot c_2 - \frac{\mathrm{Faraday}(i)}{M} \\
v &= h(c_3, \theta)
\end{aligned} \tag{1}$$

where c_1 is the concentration of the *undissolved* alumina powders; c_2 is the concentration of the *undissolved* alumina agglomerates; c_3 is the concentration of the *dissolved* alumina; k_1 is the dissolution rate constant for alumina powder; k_2 is the dissolution rate constant for alumina agglomerates; u is the overall mass of alumina addition to the whole cell; M is the mass of the bath; r is the ratio of alumina that enters the cell as alumina powder at each addition; Faraday(i) is the alumina consumption calculated based on Faraday's law and current; v is the cell voltage and θ contains the parameters in the model equation including ACD, anode resistance, bath temperature, bath ratio, AlF_3 concentration and cell designing parameters. The cell voltage equation is available in [14]. The process model above forms the basis of the equations used to develop the extended Kalman filter.

The extended Kalman filter is the most widely applied nonlinear state estimation method [15]. It can produce statistically optimal estimation of underlying variables, commonly referred to as the states, even based on the observation of noisy measurement and other modelling inaccuracies as a function of time. Furthermore, the Kalman filter employs a recursive algorithm so that the number of states can also be estimated with less number of measurements.

In order to ensure the observability, the number of states in the process needs to be reduced. Thus, the alumina dissolution mechanism is simplified. The fast and slow dissolution mechanisms represented by two first-order rate equations are combined into one first-order rate equation. The undissolved alumina, c_1 and c_2, are lumped into one parameter c_{un}; k_{un} is the effective dissolution constant for the undissolved alumina, which is a combination of k_1, k_2 and r. The discrete form of the model equation is then modified as shown below:

$$
\begin{aligned}
c_{\mathrm{un}}^{N+1} &= c_{\mathrm{un}}^{N} - \Delta t \cdot k_{\mathrm{un}} \cdot c_{\mathrm{un}}^{N} + \frac{u}{M} + \omega_1 \\
c_{\mathrm{d}}^{N+1} &= c_{\mathrm{d}}^{N} + \Delta t \cdot k_{\mathrm{un}} \cdot c_{\mathrm{un}}^{N} - \frac{\mathrm{Faraday}(i)}{M} + \omega_2 \\
ACD^{N+1} &= ACD^{N} + b + \omega_3 \\
v^{N+1} &= h\left(c_{\mathrm{d}}^{N+1}, ACD^{N+1}, \theta\right) + z
\end{aligned}
\qquad (2)
$$

where c_{un} is the concentration of the undissolved alumina; k_{un} is the effective rate constant for the dissolution; c_d is the concentration of the dissolved alumina; b is the beam movement. The process noise and modelling inaccuracies are represented by ω_1, ω_2 and ω_3, which include the mass transfer between the control volumes and inaccuracies of model parameters and the measurement noise is represented as z. It should be noted that as the cell voltage is sensitive to the variations of the ACD, this parameter also needs to be estimated.

Kalman Filter Formulation

Using a similar method described in [10], a two-stage cascaded extended Kalman filter is developed to estimate the local alumina concentration, the respective dissolution rate constant and local ACD. The schematic diagram of the structure is outlined in Figure 1.

In the first stage, the global average concentration of the dissolved and undissolved alumina, and the average rate constant for dissolution are estimated from the information of alumina addition and average ACD, line current measurements and cell voltage measurements. The estimation results are then used in the second stage of the Kalman filter.

In the second stage, the cell is discretized into subsystems. For example, if the local cell conditions near anode 1 and anode 2 are of interest, the cell can be divided into two subsystems. One subsystem contains anode 1 and anode 2, as denoted by the subscript, a, in Equation (3), while the other subsystem contains the rest of the anodes, as denoted by the subscript, b. This example is depicted in Figure 2.

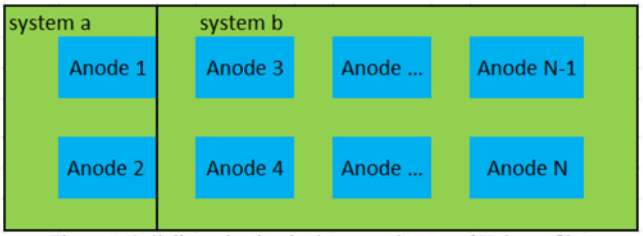

Figure 2 Cell discretization in the second stage of Kalman filter

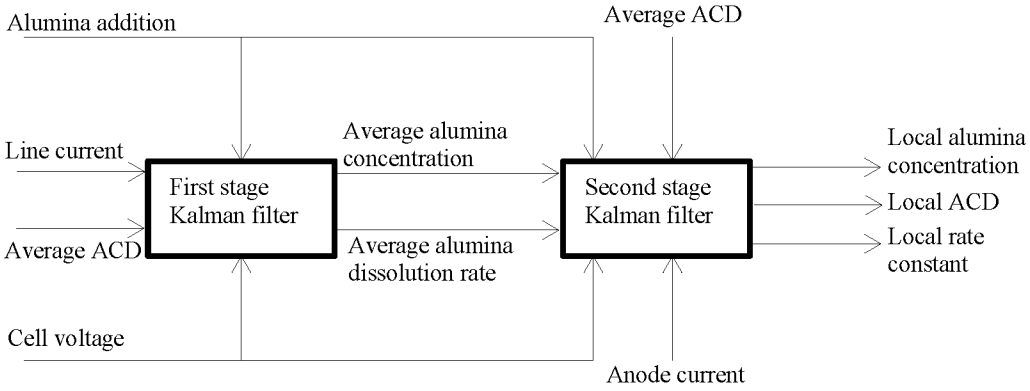

Figure 1 Structure of the cascaded Kalman filter

Thus, the additional output equation for the second stage of the Kalman filter can be written as:

$$
\begin{aligned}
c^N_{\mathrm{un}_{\mathrm{average}}} &= W_1 \left\lfloor c^N_{\mathrm{un}} \right\rfloor_{\mathrm{a}} + W_2 \left\lfloor c^N_{\mathrm{un}} \right\rfloor_{\mathrm{b}} \\
c^N_{\mathrm{d}_{\mathrm{average}}} &= W_1 \left\lfloor c^N_{\mathrm{d}} \right\rfloor_{\mathrm{a}} + W_2 \left\lfloor c^N_{\mathrm{d}} \right\rfloor_{\mathrm{b}} \\
ACD^N_{\mathrm{average}} &= W_1 ACD^N_{\mathrm{a}} + W_2 ACD^N_{\mathrm{b}} \\
c^N_{\mathrm{un}_{\mathrm{average}}} \cdot k^N_{\mathrm{un}_{\mathrm{average}}} &= W_3 \left\lfloor c^N_{\mathrm{un}} \right\rfloor_{\mathrm{a}} \left\lfloor k^N_{\mathrm{un}} \right\rfloor_{\mathrm{a}} + W_4 \left\lfloor c^N_{\mathrm{un}} \right\rfloor_{\mathrm{b}} \left\lfloor k^N_{\mathrm{un}} \right\rfloor_{\mathrm{b}}
\end{aligned}
\tag{3}
$$

where W_1, W_2, W_3 and W_4 are the weightings for each subsystem, which are dependent on the discretization of the cell, including the number of anodes and ACD in each subsystem. Equation (3) provides a constraint for the second-stage Kalman filter, which states that the global average concentration of undissolved and dissolved alumina, as well as the average ACD, should be a linear combination of the estimated values of each subsystem. Specifically, h_5 is based on the fact that the total consumption of undissolved alumina should be the sum of the consumption of undissolved alumina in each subsystem. From state-space equations (2) and (3), state estimation can be performed using the cascaded extended Kalman filter. Further information of the procedure can be referred in [10, 15].

Estimation Results and Discussion

The method described in previous sections is used to estimate the local alumina concentration and the respective local dissolution rate constant based on individual anode current measurements obtained from the experiment published in [16]. In the experiment, an additional amount of alumina was deliberately fed into the cell at 10:00 where the superheat and the alumina concentration were measured intermittently at the same location.

Estimation of local alumina concentration

The local alumina concentration is estimated from the two-stage cascaded Kalman filter described above. Figure 3 shows the estimated values of alumina concentration, which are compared with the measurements.

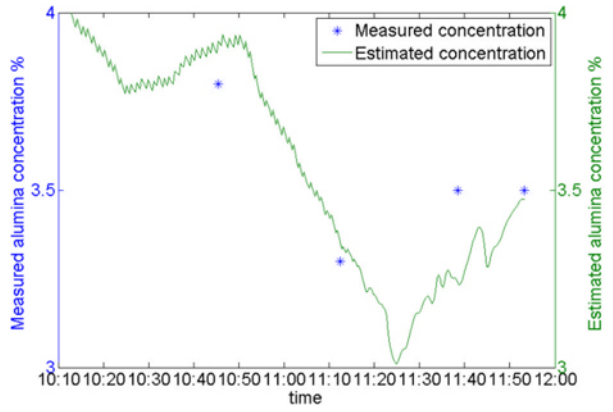

Figure 3 Comparison of estimated and measured alumina concentration

In this work, the Kalman filter is used because it has the capability to provide the statistically best estimation even based on model parameter with uncertainty, and noisy measurements. This is illustrated with the results in Figure 3, where the estimated alumina concentration generally follows the trend of the concentration measurements. The capability of the proposed Kalman filter structure is illustrated further as shown in Figure 4.

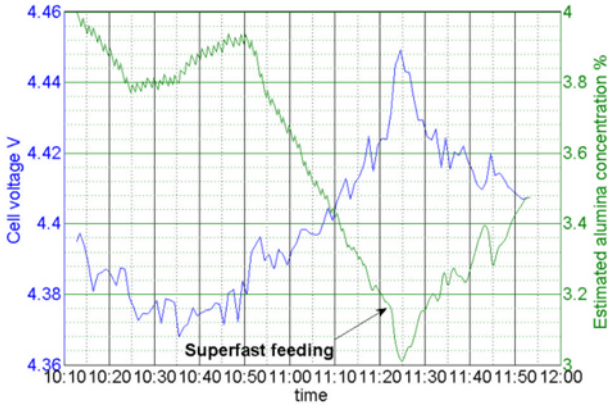

Figure 4 Comparison of cell voltage and estimated alumina concentration after the addition of extra feed

During the underfeeding (the entire period before the superfast feeding), the estimated local alumina concentration decreases as expected, and it can be seen that the concentration further decreases even right after the superfast feeding. The decrease, in fact, is consistent with the trend of the cell voltage as shown in Figure 4. As shown in Figure 4, the cell voltage reached its maximum at 11:24. As there was no beam movement, the maximum indicated that the overall alumina concentration of the cell has reached the lowest point at that period of time. However, it should be pointed out that it may not be necessary for the case of local alumina concentration. The simulation results in fact show that there exists a time difference between the maximum of the cell voltage and the minimum of the estimated local alumina concentration. This suggests that the estimation method based on individual anode currents is able to capture the spatial variations of the alumina concentration, but not only just to reflect the variations in the cell voltage or the pseudo-resistance.

Estimation of local dissolution rate constant

The respective rate constant of the local dissolution is also estimated at the same time with the alumina concentration. The result can be found in Figure 5, which is plotted with the superheat measurements.

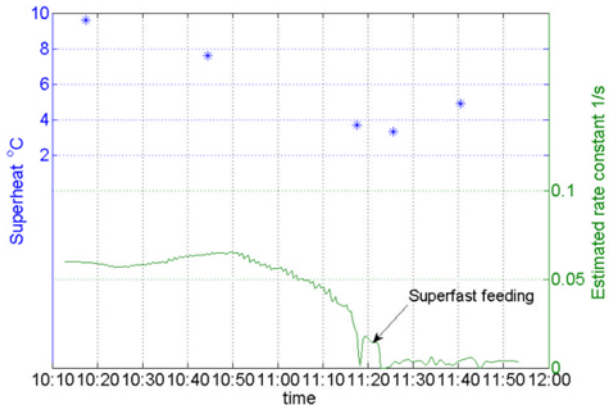

Figure 5 Comparison of superheat and estimated rate constant after additional feed introduced by the experiment

As it can be seen that the rate constant is steady initially, which is followed by a gradual decrease to almost zero, and then stays in that region until the measurement stopped. Since the cell was fed with extra amount of alumina at 10:00, there was a significant amount of undissolved alumina in the bath. The decrease in the superheat was found during the underfeed cycle, which suggests that the undissolved alumina gradually consumes the available heat for dissolution. As the estimated local rate constant is consistent with the local superheat measurements, it is reasonable to believe that the dissolution mechanism of the alumina is heat-transfer controlled and the rate constant for dissolution is largely affected by the superheat in this experiment. In addition, as shown in Figure 5, the superfast feeding and the subsequent overfeeding resulted in the further decrease in low superheat (3.3°C at 11:22), because their respective feed rates are higher than the theoretical consumption rate. This shows that the estimation method is capable of identifying low superheat resulting from different causes. Besides, based on the result, it is found that the relationship between the superheat and rate constant is not linear, i.e. higher superheat does not necessarily mean higher dissolution rate, but as shown in the estimation, the low superheat can be reflected by the slow dissolution rate. It should be noted that the undissolved alumina concentration, c_{un}, is estimated at the same time as the dissolution rate constant, which can be valuable when the undissolved alumina concentration is of interest.

Conclusion

This paper proposes a method to monitor local alumina concentration and superheat-dependent dissolution rate constant. The algorithm features a two-stage cascaded Kalman filter, which estimates the local cell conditions from individual anode current measurements, cell voltage measurements and information of alumina addition and average ACD. It has been shown that the estimated local alumina concentration matches the general trend of the measured values, whereas the rate constant of the alumina dissolution reflects local low superheat condition. The results suggest that the method is effective in monitoring the cell conditions, especially for cell operates at low superheat which is commonly in low voltage reduction cells. As the variables and parameters considered in the process model are sufficient to capture the local information of interests, which leads to possible future development for fault detection.

The advantage of using Kalman filter for state estimation is also demonstrated in this work. Accurate modelling parameters are not necessary as their uncertainties can be treated as noise. This feature is important for estimating cell conditions in the Hall-Héroult process as process parameters such as bath temperature, bath ratio and AlF_3 concentration are usually hard to determine. As they often change over time, only a rough approximation can be obtained.

To improve the efficiency and to further prove the accuracy of the method, further experiments can be carried out for further development of the method:

1. Introducing significant spatial variations and measuring alumina concentration and superheat at different locations. The measured values could then be compared with the estimation, and;
2. Measuring superheat in the cell for a long period of time with some disturbance in the energy balance. The estimated rate constant can then be correlated with the measured superheat to establish an empirical mathematical equation.

Acknowledgement

The authors wish to acknowledge the technical and financial support from Dubai Aluminum Company.

References

1. G. Bearne, "The development of aluminum reduction cell process control," *JOM Journal of the Minerals, Metals and Materials Society*, 51(1999), 16-22.

2. J. Keniry and E, Shaidulin, "Anode signal analysis: the next generation in reduction cell control," *Proceedings of TMS Light Metals*, New Orleans, LA, 2008, 287-292.

3. R. Hvidsten and K. Rye, "Practical application of the continuous measurement of individual anode current in Hall-Héroult cells," *Proceedings of TMS Light Metals*, New Orleans, LA, 2008, 329-331.

4. C.Y. Cheung et al., "Characterization of individual anode current signals in aluminum reduction cells," *Industrial & Engineering Chemistry Research*, *52*(28), (2013), 9632-9644.

5. C.Y. Cheung et al., "Spatial temperature profiles in an aluminum reduction cell under different anode current distributions," *AIChE Journal, 59*(5), (2012), 1544-1556.

6. E. Batista et al., "Statistical method to predict anode effect events," *Proceedings of the 19th International Symposium of ICSOBA*, Belém, Brazil, 2012.

7. S.R. Jakobsen et al., "Estimating alumina concentration distribution in aluminum electrolysis cells", *Proceedings of IFAC automation in mining, mineral and metal processing*, Tokyo, Japan, 2001, 303-308.

8. K. Hestetun and M. Hovd, "Detecting abnormal feed rate in aluminum electrolysis using extended Kalman filter," *Proceedings of the 16th IFAC World Congress*, Czech Republic, 2005, 85-90.

9. K. Hestetun and M. Hovd, "Detection of abnormal alumina feed rate in aluminum electrolysis cells using stat and parameter estimation," *Proceedings of the 16th European Symposium on Computer Aided Process Engineering and 9th International Symposium on Process Systems Engineering,* Garmisch-Partenkirchen, Germany, 2006, 1557-1562.

10. Y. Yao et al., "Process monitoring in aluminium reduction cells via state estimation", *11th AustralAsian Aluminum Smelting Technology Conference*, 2014

11. G.I. Kuschel and B.J. Welch, "Further studies of alumina dissolution under conditions similar to cell operation", *Proceedings of TMS Light Metals*, New Orleans, LA, 1991, 112-118

12. R.G. Haverkamp and B.J. Welch, "Modelling the dissolution of alumina powder in cryolite," *Chemical Engineering and Processing*, 37(1998), 177-187.

13. P. Biedler, "Modeling of an aluminum reduction cell for the development of a state estimator," (Ph.D Thesis, West Virginia University, 2003), 82

14. W. Haupin, "Interpreting the components of cell voltage," *Proceedings of TMS Light Metals*, Warrendale, PA, 1998, 531-537.

15. D. Simon, *Optimal state estimation-Kalman, H_∞ , and nonlinear approaches* (Hoboken, New Jersey, John Wiley & Sons, 2006), 395-428.

16. C.Y. Cheung, "Anode current signals analysis, characterization and modelling of aluminum reduction cells," (Ph.D Thesis, University of New South Wales, 2013), 109-111.